Differential Regulation of Hepatic Macrophage Fate by Chi3l1 in MASLD

Jia He[1], Bo Chen[1], Xiong Wang[1], Ruoxue Yang[1], Chengxiang Deng[1], Xiane Zhu[1], Keqin Wang[1], Lang Wang[1], Xiaokang Lu[2], Cheng Peng[1], Canpeng Li[2], Zhao Shan[1]*

1. Yunnan Key Laboratory of Cell Metabolism and Diseases, Center for Life Sciences, School of Life Sciences, Kunming, China, 650500*Corresponding author
2. School of Chemical Science and Technology, Yunnan University, Kunming, China, 650500

*email: Zhao Shan: shanzhao@ynu.edu.cn

Declaration of interests
The authors declare no competing interests.

Financial Support
Supported by National Natural Science Foundation of China (32071129 to Z.S.), Yunnan Provincial Science and Technology Department (C619300A086 to Z.S.).

Author Contributions
JH conducted the experiments, analyzed the data, and wrote the manuscript. BC performed the analysis of single-cell RNA sequencing (sc-RNA-seq) data and wrote the manuscript. WX was involved in the care and feeding of the mice. RXY helped preparation of the sc-RNA-seq library. CXD conducted the initial analysis of the sc-RNA-seq data under the supervision of CP. XEZ participated in sample collection. KQW and LW were responsible for purifying the recombinant Chi3l1 protein. CPL and XKL assisted in synthesizing biotin-labeled glucose. ZS conceived, organized, and designed the study, and wrote the manuscript.

Abstract

Metabolic dysfunction-associated steatotic liver disease (MASLD) progression involves the replacement of protective embryo-derived Kupffer cells (KCs) by inflammatory monocyte-derived macrophages (MoMFs), yet the regulatory mechanisms remain unclear. Here, we identify chitinase 3-like 1 (Chi3l1/YKL-40) as a critical metabolic regulator of hepatic macrophage fate. We observed high expression of Chi3l1 in both KCs and MoMFs during MASLD development. Genetic deletion of Chi3l1 specifically in KCs significantly exacerbated MASLD severity and metabolic dysfunction, whereas MoMF-specific Chi3l1 deletion showed minimal metabolic effects. Mechanistic studies revealed that this cell type-specific regulation arises from differential metabolic requirements: KCs display elevated glucose metabolism compared to MoMFs. Chi3l1 directly interacts with glucose to inhibit its cellular uptake, thereby selectively protecting glucose-dependent KCs from metabolic stress-induced cell death while having negligible effects on less glucose-dependent MoMFs. These findings uncover a novel Chi3l1-mediated metabolic checkpoint that preferentially maintains KCs populations through glucose metabolism modulation, providing important new insights into the pathogenesis of MASLD and potential therapeutic strategies targeting macrophage-specific metabolic pathways.

Key words: Kupffer cells, Monocytes-derived macrophages, MASLD, Chi3l1

Introduction

Metabolic dysfunction-associated steatotic liver disease (MASLD) has become the most prevalent chronic liver disorder in western populations, affecting approximately 30% of adults and driven by its strong association with obesity and metabolic syndrome[1]. The disease spectrum ranges from matabolic dysfunction-associated fatty liver (MAFL) to metabolic dysfunction-associated steatohepatitis (MASH), with the latter characterized by steatosis, inflammation, hepatocyte ballooning, and progressive fibrosis[2]. Central to MASLD pathogenesis are hepatic macrophages, particularly the embryo-derived Kupffer cells (KCs) that reside in liver sinusoids[3,4]. These self-renewing resident macrophages[5], play crucial roles in lipid homeostasis, as evidenced by studies showing that depletion of $CD207^{+}$ KCs leads to impaired triglyceride storage[6]. When KCs die during MASH progression, they are gradually replaced by monocyte-derived macrophages (MoMFs) that exhibit more inflammatory properties and contribute to liver injury[6,7].This transition from protective embryo-derived KCs (EmKCs) to inflammatory monocyte-derived KCs (MoKCs) represents a critical juncture in disease progression, yet the mechanisms regulating this shift remain poorly understood.

A key determinant of macrophage function is cellular metabolism. Macrophages dynamically switch between glycolytic and oxidative phosphorylation pathways to adapt to environmental changes[8]. During MASLD, hepatic macrophages increase their glycolytic activity, which may exacerbate inflammation and tissue damage[9-11]. While glucose metabolism is known to influence macrophage polarization, its specific role in determining hepatic macrophage fate - particularly the balance between KCs and MoMFs - remains unknown. Chitinase 3-like 1 (Chi3l1/YKL-40) has emerged as an important regulator of macrophage biology, promoting cell survival through ERK1/2 and PI3K/Akt pathways while modulating anti-inflammatory cytokines like IL-10[12-16]. However, its potential role in macrophage metabolic reprogramming, particularly in the context of hepatic glucose metabolism, has not been explored.

In this study, we identify a novel mechanism by which Chi3l1 governs hepatic macrophage fate through metabolic regulation. We demonstrate that Chi3l1 directly interacts with glucose to suppress its uptake in macrophages. Strikingly, this interaction selectively protects glucose-high KCs from cell death in MASLD conditions, while having minimal effect on glucose-low MoMFs. These findings reveal a previously unrecognized Chi3l1-mediated metabolic checkpoint that maintains KC populations, providing new insights into the pathogenesis of MASLD and potential therapeutic strategies.

Materials and methods

Animal experiments and procedures

Animals *Chil1*$^{-/-}$ (strain no. T014402), *Chil1*$^{flox//flox}$ (strain no. T013652), *Lyz2-cre* (strain no. T003822) and *Clec4f-cre* (strain no. T036801) mice with a *C57BL/6J* background were purchased from GemPharmatech. *Rosa tdtomato* mice (strain no. C001181) were purchased from Cyagen. Accordingly, *C57BL/6J* mice (strain no. N000013) were used as wild-type (WT) mice. To generate *Clec4f*$^{\Delta Chil1}$ mice, *Chil1*$^{flox//flox}$ mice were crossed with *Clec4f-cre* mice and knock out efficiency was

examined in KCs by qRT-PCR (Figure S2B). To generate *Clec4f*$^{Rosa\ tdtomato}$ mice, *Rosa tdtomato* mice were crossed with *Clec4f-cre* mice to examine the expression specificity of *Clec4f-cre* (Figure S2C). To generate *Lyz2*$^{\triangle Chil1}$ mice, *Chil1*$^{flox//flox}$ mice were crossed with *Lyz2-cre* mice and knock out efficiency was examined in BMDM by western blot (Figure S3B). All mouse colonies were maintained at the Animal Core Facility of Yunnan University. The animal studies were approved by the Yunnan University Institutional Animal Care and Use Committee (IACUC, Approval No. YNU20220314). Male mice aged 6-8 weeks were used in this study.

Construction of MASLD/MASH mouse model Mice were provided a high-fat and high-cholesterol diet (Research Diet, d12108c, 40 kcal% fat and 1.25% cholesterol). Throughout the feeding period, the body weight and food consumption of the mice were observed and recorded weekly. Once the dietary intervention was completed, the mice were euthanized. Liver and murine serum samples were collected for further analysis. Alanine aminotransferase (ALT) and aspartate aminotransferase (AST) levels in the serum, as well as cholesterol (TC) and triglyceride (TG) levels in both serum and liver tissues, were quantified using commercially available kits (Nanjing Jiancheng Bioengineering Institute).

Statistical analysis

Data are presented as mean ± standard error of the mean (SEM) in all graph figures. Statistical analyses were conducted using the SPSS statistics software (Version 22). To compare the two groups, an unpaired two-tailed Student's t-test was used. One-way analysis of variance (ANOVA) was performed for comparisons involving three or more groups. For patients with MASLD liver, the samples were tested using the Mann-Whitney test. Statistical significance was set at $p < 0.05$ and p value is indicated. All cell culture results represent at least three independent experiments.

Additional Methods

Additional detailed methods can be found in the Supporting Information.

Results

Hepatic macrophages express Chi3l1.

To investigate the dynamic changes in hepatic macrophages, we performed BD Rhapsody scRNA-seq on non-parenchymal cells (NPCs) isolated from healthy livers of mice fed a normal chow diet (NCD) and from livers of mice with MASLD induced by a high-fat, high-cholesterol (HFHC) diet. After quality control and filtration, we retained 23,312 cells from NCD livers and 6,567 cells from HFHC livers for downstream analysis. Using a graph-based clustering approach, we identified 32 distinct cell populations, visualized via uniform manifold approximation and projection (UMAP) (Figure 1A). Monocyte/macrophage subsets were further defined based on lineage-specific markers: Monocytes expressed *Ly6c2, Chil3, S100a6, Ccr2, Itgam*, and *Cx3cr1* but lacked macrophage markers. KCs were marked by *Cd68, Vsig4, Clec4f, Timd4, Adgre1*, and *Clec1b*. MoMFs were negative for KCs markers but positive for macrophage markers such as *Ccr2, Cx3cr1, Cd9, Itgax, Gpnmb, Cd68,* and *Adgre1* (Figure 1B, C; UMAP in Fig S1A)[17,18]. ScRNA-seq analysis revealed high expression of *Chil1* (*Chil1* being the gene name for Chi3l1) in hepatic macrophages (Figure 1D). To validate this, we performed immunofluorescence staining for Chi3l1 in hepatic macrophages using antibodies against Timd4, F4/80, and Chi3l1. Our results confirmed Chi3l1

expression in hepatic macrophages under both NCD and HFHC conditions (Figure 1E). Consistently, patients with MAFL or MASH exhibited elevated hepatic *Chil1* mRNA levels, which correlated with MASLD severity and fibrosis stage (Figure 1F, G). These findings suggest that Chi3l1 is expressed in hepatic macrophages and may play a role in MASLD progression.

Deficiency of Chi3l1 in Kupffer cells promotes insulin resistance and hepatic lipid accumulation.

Given that hepatic macrophages are the primary source of Chi3l1 in the liver, we investigated its functional role by generating mice with conditional knockout (cKO) of *Chil1* in either KCs or MoMFs. First, we generated *Clec4f* $^{\Delta Chil1}$ mice by crossing Chil1$^{fl/fl}$ mice with *Clec4f-cre* mice[19], achieving selective Chil1 ablation in KCs (Figure S2A). When fed an HFHC diet, *Clec4f*$^{\Delta Chil1}$ mice exhibited: Increased hepatic lipid deposition, evident by H&E and Oil Red O staining as early as 8 weeks (Figure 2A, B). Elevated metabolic disturbances at 16 weeks, including higher liver index (liver/body weight), serum ALT, and increased cholesterol/triglycerides in both liver and serum (Figure 2C). Impaired glucose metabolism, with worsened glucose tolerance (IGTT) and insulin resistance (ITT) (Figure 2D, E). These results demonstrate that Chi3l1 deficiency in KCs drives lipid accumulation and insulin resistance.

To assess the role of Chi3l1 in MoMFs, we generated *Lyz2*$^{\Delta Chil1}$ mice (*Chil1*$^{fl/fl}$ × *Lyz2-Cre*[19]) (Figure S3A). After 20 weeks on an HFHC diet: Hepatic lipid accumulation (H&E, Oil Red O) was comparable to controls (Figure S4A, B). Metabolic parameters (liver index, ALT, serum/liver lipids) showed no significant differences (Figure S4C). *Lyz2*$^{\Delta Chil1}$ mice showed glucose intolerance (IGTT) but normal insulin sensitivity (ITT) (Figure S4D, E). Thus, Chi3l1 loss in MoMFs does not substantially contribute to metabolic dysregulation.

ScRNA-seq reveals upregulated glucose metabolism-related transcripts in KCs, correlating with cell death signatures.

To dissect the distinct metabolic and functional profiles between KCs and MoMFs during MASLD progression, we analyzed our scRNA-seq data. Consistent with prior studies[6,7], we observed decreased KCs numbers but increased MoMFs and monocytes in HFHC-fed mice compared to NCD controls (Figure 3A). Kyoto Encyclopedia of Genes and Genomes (KEGG) pathway analysis showed that while both cell types exhibited activation of phagocytosis-related pathways (lysosome, phagosome, endocytosis, and efferocytosis), they displayed divergent cell fate patterns (Figure 3B). KCs showed strong cell death signatures, whereas MoMFs maintained proliferative activity without evidence of cell death (Figure 3B). Monocytes showed strong cell death and proliferative activity (Figure 3B). Given the significant role of metabolic regulation in cell fate,[20] we compared pathways involved in glucose metabolism, cell death, and cell proliferation (Figure 3C). Notably, glucose metabolism pathways were significantly more active in KCs and monocytes compared to MoMFs (Figure 3C). Moreover, the cell proliferation pathway was highly activated in monocytes and consistently activated in MoMFs but not in KCs (Figure 3C). Gene Set Variation Analysis (GSVA)-based correlation analysis revealed a striking association between glucose metabolism and cell death pathways (Figure 3D). These findings demonstrate distinct glucose metabolic activation patterns between KCs and MoMFs, which may underlie their divergent cell fates in MASLD progression.

Chi3l1 deficiency promote KCs death during MASLD.

To investigate the role of Chi3l1 in KCs survival during MASLD, we generated *Chil1*$^{-/-}$ mice, as Chi3l1 is a secreted protein[21,22]. The successful knockout was confirmed by qRT-PCR analysis of liver tissue (Figure S5A, B). We then performed scRNA-seq on NPCs isolated from *Chil1*$^{-/-}$ mice fed an HFHC diet for 16 weeks. After quality control, 6,813 high-quality cells were retained for analysis. Using established KC markers (Figure 1C), we conducted GSVA to examine metabolic pathways. This revealed enhanced cell death pathways in KCs from HFHC-fed mice, with significantly greater apoptosis signatures in *Chil1*$^{-/-}$ KCs compared to wild-type (WT) controls (Figure 4A). The increased apoptosis was further supported by upregulation of pro-apoptotic genes in *Chil1*$^{-/-}$ KCs (Figure 4B).

Flow cytometry analysis validated these findings, using the gating strategy shown in Figure S6A. While WT and *Chil1*$^{-/-}$ mice showed similar KC numbers at baseline, dramatic differences emerged during HFHC feeding. WT KC numbers remained stable at 8 weeks but decreased by 50% at 16 weeks. In contrast, *Chil1*$^{-/-}$ mice exhibited accelerated KCs loss, with a 30% reduction by 8 weeks progressing to 60% by 16 weeks (Figure 4C, D). Notably, MoMFs populations remained comparable between groups at early timepoints but showed greater reduction in *Chil1*$^{-/-}$ mice at 16 weeks (Figure 4C, D).

Histological analysis through Clec4f/TUNEL co-staining provided further confirmation. While WT livers showed no TUNEL^{+} KCs at baseline, 40% were TUNEL^{+} by 8 weeks, increasing to 55% at 16 weeks. *Chil1*$^{-/-}$ mice displayed elevated KC apoptosis even at baseline, with significantly more TUNEL+ KCs (approximately 2-fold higher than WT) by 8 weeks (Figure 4E). Together, these results demonstrate that Chi3l1 deficiency accelerates HFHC-induced KCs death, leading to premature KCs depletion during MASLD progression.

Molecular interaction between Chi3l1 and glucose.

Our investigation into Chi3l1-mediated KCs survival revealed an unexpected structural relationship: Chi3l1 binds to glucose, which is structurally analogous to chitin, a polysaccharide well known to bind Chi3l1(Figure 5A). Bioinformatics analysis using the STITCH database further supported this observation, predicting a high probability of direct Chi3l1-glucose interaction (Figure 5B). To experimentally validate this interaction, we performed pull-down assays using biotin-labeled glucose incubated with plasma from HFHC-fed mice. Streptavidin bead isolation followed by anti-Chi3l1 Western blotting demonstrated specific binding between Chi3l1 and biotin-glucose, but not biotin alone (Figure 5C, D). This interaction was competitively inhibited by unlabeled glucose, confirming specificity (Figure 5D). Quantitative analysis using microscale thermophoresis with recombinant mouse Chi3l1 (rChi3l1) yielded a dissociation constant (Kd) of 4.95 mM for the Chi3l1-glucose interaction (Figure 5E). Notably, circulating Chi3l1 levels were significantly elevated in serum from HFHC-fed mice compared to baseline (Figure 5F), suggesting a potential physiological role for this interaction in metabolic regulation. These findings establish Chi3l1 as a novel glucose-binding protein that may participate in glucose homeostasis during MASLD progression.

Chi3l1 limits glucose uptake and protects hepatic macrophages from cell death.

To elucidate the functional consequences of Chi3l1-glucose binding, we examined glucose metabolism in hepatic macrophages. Using the fluorescent glucose analog 2-NBDG[23], we performed uptake assays in KCs following 12-hour glucose starvation. While glycogen droplet size remained unchanged in untreated KCs regardless of rChi3l1 supplementation (Figure 6A), 2-NBDG exposure significantly increased glycogen accumulation. This effect was markedly suppressed by rChi3l1 co-treatment (Figure 6A), a phenotype replicated in BMDM (Figure 6B). These results demonstrate that Chi3l1 restricts glucose uptake and subsequent glycogen storage.

Further validation using Stbd1 (a glycogen-binding protein[23]) immunofluorescence revealed minimal glycogen foci in glucose-deprived BMDM, with no rChi3l1-dependent differences. High-glucose conditions, however, triggered robust glycogen aggregation, which was significantly attenuated by rChi3l1 (Figure 6C). Concordantly, extracellular acidification rate (ECAR) measurements showed reduced basal and total glycolytic capacity in rChi3l1-treated BMDMs (Figure 6D,E), confirming Chi3l1's role in limiting glucose metabolism.

To test whether Chi3l1-glucose binding influence cell survival, we employed a palmitic acid (PA)-induced lipotoxicity cell-based model to better mimic the *in vivo* environment. rChi3l1 supplementation reduced PA-induced cleavage of caspase-3 (Figure 6F) and decreased KCs death (calcein/PI staining, Figure 6G). These findings collectively establish that Chi3l1 safeguards KCs by modulating glucose uptake, thereby suppressing metabolic stress-induced death.

Discussion

Our findings establish Chi3l1 as a critical metabolic regulator that controls hepatic macrophage fate through a novel glucose-dependent mechanism in MASLD. Using cell-specific knockout models, we uncovered a fundamental dichotomy in Chi3l1 function: selective ablation in KCs dramatically accelerated MASLD progression and metabolic dysfunction, whereas deletion in MoMFs produced minimal metabolic effects. Single-cell transcriptomics revealed the molecular basis for this cell-type specificity - KCs exhibit a glucose-hungry metabolic phenotype that renders them uniquely dependent on Chi3l1-mediated regulation, while MoMFs maintain a relatively glucose-independent metabolic program. At the mechanistic level, we demonstrate that Chi3l1 functions as a physiological glucose sensor, directly binding extracellular glucose to limit its cellular uptake. This interaction establishes a crucial metabolic safeguard that specifically protects glucose-dependent KCs from lethal metabolic stress while sparing glucose-independent MoMFs. Through this precise modulation of glucose availability, Chi3l1 maintains metabolic homeostasis and preserves KCs populations during chronic dietary challenge (Figure 7).

Our study reveals fundamental differences in metabolic requirements between hepatic macrophage subsets that provide new insights into MASLD pathogenesis. We demonstrate that KCs and MoMFs play stage-specific roles in disease progression, with KCs serving as critical regulators of early metabolic homeostasis while MoMFs appear more involved in later inflammatory phases. This temporal specialization explains the striking dichotomy observed in our genetic models - KCs-specific Chi3l1 deletion dramatically exacerbated metabolic dysfunction, whereas MoMFs deletion showed minimal effects. The heightened glucose metabolism of KCs during MASLD renders them uniquely vulnerable to dietary stress. Chi3l1 serves as a crucial metabolic buffer in this context,

directly protecting KCs through glucose modulation as evidenced by reduced glycogen accumulation and attenuated glycolytic flux. Our findings using the HFHC model complement previous findings in fibrogenic CDAA-HFAT models[24] or MCD/CCL4 models[25] or human livers[26], collectively suggesting Chi3l1 may have dual roles in MASLD - maintaining metabolic balance through KCs in early disease while potentially influencing fibrogenesis via MoMFs in advanced stages. The accelerated KCs death in knockout models provides direct experimental evidence linking macrophage survival to metabolic outcomes, resolving key questions about MASLD progression mechanisms.

The structural characteristics of Chi3l1 have been extensively studied. Chi3l1 is a homodimeric protein composed of two identical subunits. Each subunit consists of a catalytic domain and a carbohydrate-binding domain. The catalytic domain contains an active site capable of hydrolyzing chitin, a polymer of N-acetylglucosamine[27,28]. The carbohydrate-binding domain is responsible for the interaction between Chi3l1 and various carbohydrate ligands[27]. It is likely that Chi3l1 also interacts with glucose through its carbohydrate-binding domain. However, the precise molecular interactions between Chi3l1 and glucose are still not fully elucidated, and further research is needed to explore these interactions in greater detail. Furthermore, our data demonstrated that Chi3l1 is upregulated in the serum of mice fed a high-fat, high-cholesterol (HFHC) diet for 16 weeks (Fig. 3H). However, continuing to feed the mice for 24 weeks did not further increase the level of Chi3l1 (data not shown). This suggests that the level of Chi3l1 initially increases but reaches a plateau stage over time. These findings indicate that while Chi3l1 has the capability to bind with glucose, this interaction may be limited in living organisms.

Our findings carry important translational potential for MASLD treatment. The discovery of Chi3l1's glucose-sensing function in KCs suggests two complementary therapeutic strategies: first, developing Chi3l1-based interventions to preserve KC populations during early metabolic dysfunction; second, creating cell-type-specific approaches that selectively modulate glucose metabolism in KCs while sparing MoMFs. The structural mapping of Chi3l1's glucose-binding domain now enables rational design of small molecule mimetics to therapeutically enhance this protective pathway. Besides, several key questions emerge for future research to advance these therapeutic possibilities: (1) How glucose levels are coordinated with other death inducers such as lipid toxicity; (2) Whether competing carbohydrate ligands modulate Chi3l1's glucose-sensing capacity in different metabolic states; (3) The clinical relevance of human Chi3l1 variants in MASLD susceptibility and progression. Addressing these questions will be crucial for translating our mechanistic insights into targeted therapies that account for the complex metabolic specialization of hepatic macrophage subsets.

Our findings reveal a novel metabolic checkpoint in which Chi3l1 selectively sustains KCs populations by modulating glucose metabolism, offering key insights into MASLD pathogenesis. The study highlights the therapeutic potential of targeting Chi3l1-glucose interactions to preserve protective KCs and curb MASLD progression. Future research should explore whether Chi3l1 supplementation or pharmacological modulation can rescue KCs viability, as well as investigate whether this mechanism extends to other macrophage-driven metabolic disorders, such as MASH or diabetes. By identifying cell type-specific metabolic vulnerabilities, this work paves the way for

precision therapies that selectively manipulate macrophage subsets to treat liver disease.

Abbreviations

MASLD, metabolic dysfunction-associated steatotic liver disease; MASH, metabolic dysfunction-associated steatohepatitis; KCs, Kupffer cells; Chi3l1, Chitinase 3 like 1; ERK1/2, extracellular signal-regulated kinase 1/2; PI3K, phosphoinositide-3 kinase; ALT, Alanine aminotransferase; AST, aspartate aminotransferase; TC, cholesterol; TG, triglyceride; NPCs, nonparenchymal cells; HFHC, high fat high cholesterol diet; NCD, normal chow diet; Clec4f, C-type lectin domain family 4; Timd-4,T cell immunoglobulin mucin protein 4; MoMFs, monocyte-derived macrophages; HFD, high-fat diet; MCD, methionine/choline deficient diet; WD, western diet; PPP, pentose phosphate pathway; BMDM, bone marrow derived macrophages; DMSO, dimethyl sulfoxide; MAFL, non-alcoholic fatty liver; rChi3l1, recombinant murine Chi3l1; PA, palmic acid; Iso, Isopropyl alcohol; IGTT, intraperitoneal glucose tolerance test; ITT, insulin tolerance test; scRNA-seq, single-cell RNA sequencing; MoKCs, monocytes-derived Kupffer cells; ALD, alcohol-induced liver disease; AILI, acetaminophen-induced liver injury; EmKCs, embryo-derived Kupffer cells; MASH, metabolic dysfunction-associated steatohepatitis; DT, diphtheria toxin; WT, wild-type; Tunel, TdT-mediated dUTP Nick-End Labeling;

Acknowledgements

We thank Dr. Bin Qi (Yunnan University) for suggestions and discussion. We thank Guangxun Meng (The Shanghai Institute of Immunity and Infection of the Chinese Academy of Sciences) for providing us with L929 cells. We thank Cynthia Ju (UTHealth) for advice in manuscript submission.

Reference

1 Hardy, T., Oakley, F., Anstee, Q. M. & Day, C. P. Nonalcoholic Fatty Liver Disease: Pathogenesis and Disease Spectrum. *Annu Rev Pathol-Mech* **11**, 451-496, doi:10.1146/annurev-pathol-012615-044224 (2016).

2 Eslam, M. *et al.* A new definition for metabolic dysfunction-associated fatty liver disease: An international expert consensus statement. *Journal of Hepatology* **73**, 202-209, doi:10.1016/j.jhep.2020.03.039 (2020).

3 Kazankov, K. *et al.* The role of macrophages in nonalcoholic fatty liver disease and nonalcoholic steatohepatitis. *Nature reviews. Gastroenterology & hepatology* **16**, 145-159, doi:10.1038/s41575-018-0082-x (2019).

4 Gomez Perdiguero, E. *et al.* Tissue-resident macrophages originate from yolk-sac-derived erythro-myeloid progenitors. *Nature* **518**, 547-551, doi:10.1038/nature13989 (2015).

5 Hashimoto, D. *et al.* Tissue-Resident Macrophages Self-Maintain Locally throughout Adult Life with Minimal Contribution from Circulating Monocytes. *Immunity* **38**, 792-804, doi:10.1016/j.immuni.2013.04.004 (2013).

6 Tran, S. *et al.* Impaired Kupffer Cell Self-Renewal Alters the Liver Response to Lipid Overload during Non-alcoholic Steatohepatitis. *Immunity* **53**, 627-640.e625, doi:10.1016/j.immuni.2020.06.003 (2020).

7 Daemen, S. *et al.* Dynamic Shifts in the Composition of Resident and Recruited Macrophages Influence Tissue Remodeling in NASH. *Cell Rep* **34**, 108626, doi:10.1016/j.celrep.2020.108626 (2021).

8 Green, D. R., Galluzzi, L. & Kroemer, G. Cell biology. Metabolic control of cell death. *Science* **345**, 1250256, doi:10.1126/science.1250256 (2014).

9 Inomata, Y. *et al.* Downregulation of miR-122-5p Activates Glycolysis via PKM2 in Kupffer Cells of Rat and Mouse Models of Non-Alcoholic Steatohepatitis. *International journal of molecular sciences* **23**, doi:10.3390/ijms23095230 (2022).

10 Lodge, M. *et al.* Fructose regulates the pentose phosphate pathway and induces an inflammatory and resolution phenotype in Kupffer cells. *Sci Rep-Uk* **14**, doi:ARTN 402010.1038/s41598-024-54272-w (2024).

11 Dong, T. *et al.* Activation of GPR3-β-arrestin2-PKM2 pathway in Kupffer cells stimulates glycolysis and inhibits obesity and liver pathogenesis. *Nature Communications* **15**, doi:ARTN 80710.1038/s41467-024-45167-5 (2024).

12 Lee, C. G. *et al.* Role of chitin and chitinase/chitinase-like proteins in inflammation, tissue remodeling, and injury. *Annual review of physiology* **73**, 479-501, doi:10.1146/annurev-physiol-012110-142250 (2011).

13 Dela Cruz, C. S. *et al.* Chitinase 3-like-1 promotes Streptococcus pneumoniae killing and augments host tolerance to lung antibacterial responses. *Cell host & microbe* **12**, 34-46, doi:10.1016/j.chom.2012.05.017 (2012).

14 He, C. H. *et al.* Chitinase 3-like 1 regulates cellular and tissue responses via IL-13 receptor α2. *Cell reports* **4**, 830-841, doi:10.1016/j.celrep.2013.07.032 (2013).

15 Zhou, Y. *et al.* Chitinase 3-like-1 and its receptors in Hermansky-Pudlak syndrome-associated lung disease. *The Journal of clinical investigation* **125**, 3178-3192, doi:10.1172/jci79792 (2015).

16 Lee, C. G. *et al.* Role of breast regression protein 39 (BRP-39)/chitinase 3-like-1 in Th2 and IL-13-induced tissue responses and apoptosis. *J Exp Med* **206**, 1149-1166, doi:10.1084/jem.20081271 (2009).

17 Li, L. *et al.* Kupffer-cell-derived IL-6 is repurposed for hepatocyte dedifferentiation via activating progenitor genes from injury-specific enhancers. *Cell Stem Cell* **30**, 283-+, doi:10.1016/j.stem.2023.01.009 (2023).

18 Seidman, J. S. *et al.* Niche-Specific Reprogramming of Epigenetic Landscapes Drives Myeloid Cell Diversity in Nonalcoholic Steatohepatitis. *Immunity* **52**, 1057-+, doi:10.1016/j.immuni.2020.04.001 (2020).

19 Scott, C. L. *et al.* The Transcription Factor ZEB2 Is Required to Maintain the Tissue-Specific Identities of Macrophages. *Immunity* **49**, 312-325 e315, doi:10.1016/j.immuni.2018.07.004 (2018).

20 Green, D. R., Galluzzi, L. & Kroemer, G. Metabolic control of cell death. *Science* **345**, 1466-+, doi:ARTN 125025610.1126/science.1250256 (2014).

21 Shan, Z. *et al.* Chitinase 3-like-1 contributes to acetaminophen-induced liver injury by promoting hepatic platelet recruitment. *Elife* **10**, doi:10.7554/eLife.68571 (2021).

22 Shan, Z. *et al.* Chitinase 3-like-1 promotes intrahepatic activation of coagulation through induction of tissue factor in mice. *Hepatology* **67**, 2384-2396, doi:10.1002/hep.29733 (2018).

23 Liu, Q. X. *et al.* Glycogen accumulation and phase separation drives liver tumor initiation. *Cell* **184**, 5559-+, doi:10.1016/j.cell.2021.10.001 (2021).

24 Kim, A. D. *et al.* Myeloid-specific deletion of chitinase-3-like 1 protein ameliorates murine

diet-induced steatohepatitis progression. *J Mol Med* **101**, 813-828, doi:10.1007/s00109-023-02325-4 (2023).

25 Higashiyama, M. *et al.* Chitinase 3-like 1 deficiency ameliorates liver fibrosis by promoting hepatic macrophage apoptosis. *Hepatology Research* **49**, 1316-1328, doi:10.1111/hepr.13396 (2019).

26 Nishimura, N. *et al.* Chitinase 3-like 1 is a profibrogenic factor overexpressed in the aging liver and in patients with liver cirrhosis. *P Natl Acad Sci USA* **118**, doi:ARTN e201963311810.1073/pnas.2019633118 (2021).

27 Fusetti, F., Pijning, T., Kalk, K. H., Bos, E. & Dijkstra, B. W. Crystal structure and carbohydrate-binding properties of the human cartilage glycoprotein-39. *Journal of Biological Chemistry* **278**, 37753-37760, doi:10.1074/jbc.M303137200 (2003).

28 Houston, D. R., Recklies, A. D., Krupa, J. C. & van Aalten, D. M. F. Structure and ligand-induced conformational change of the 39-kDa glycoprotein from human articular chondrocytes. *Journal of Biological Chemistry* **278**, 30206-30212, doi:10.1074/jbc.M303371200 (2003).

Main figure

Figure 1. Hepatic macrophages express Chi3l1.

(A-D) Wildtype C57BL/6J mice were fed either a normal chow diet (NCD) or HFHC for 16 weeks. NPCs were isolated and subjected to BD Rhapsody scRNA sequencing.

(A) Uniform manifold approximation and projection (UMAP) plots illustrate the clustering of NPCs in the livers of mice fed NCD and HFHC. Cell clusters are color-coded, with monocytes/macrophages clusters outlined.

(B) UMAP plots depict the clustering of Monocytes/Macrophages in the livers of mice fed NCD and HFHC. Cell clusters are color-coded.

(C) Dot plot displays the scaled gene expression levels of lineage-specific marker genes in different cell clusters.

(D) Dot plot shows the scaled gene expression levels of Chil1 in the indicated cell clusters.

(E) Immunofluorescent staining of Timd4 (white), F4/80 (red), Chi3l1 (green), and nuclear DAPI (blue) in liver sections of mice fed with either NCD or HFHC for 16 weeks, illustrating Chi3l1 expression in hepatic macrophages. Scale bar=20μm and 5μm (zoom).

(G) mRNA expression levels of Chil1 in liver tissues of patients with metabolic dysfunction-associated fatty liver (MAFL) or with metabolic dysfunction-associated steatohepatitis (MASH) (GEO Datasets: GSE167523, GSE207310, GSE130970). No-MAFLD or Healthy individuals serve as controls.

(H) The correlation between mRNA expression levels of Chil1 and MASLD activity score or fibrosis stage was analyzed (GEO Datasets: GSE130970).

Representative images were shown in E. Mann-Whitney test was performed in F. Pearson's correlation was performed in G. P value and r value are as indicated.

Figure 2. Deficiency of Chi3l1 in Kupffer cells promotes insulin resistance and hepatic lipid accumulation.

Chil1$^{fl/fl}$ and *Clec4f*$^{\Delta Chil1}$ mice were fed with a HFHC diet for 0, 8 and 16 weeks.

(A) H&E staining was performed to examine liver histology of *Chil1*$^{fl/fl}$ and *Clec4f*$^{\Delta Chil1}$ mice fed

the HFHC diet for 0, 8 and 16 weeks. Scale bar=20μm.

(B) Oil red o staining was performed to detect fat accumulation in the livers of *Chil1*$^{fl/fl}$ and *Clec4f*$^{\Delta Chil1}$ mice fed the HFHC diet for 0, 8 and 16 weeks. Scale bar=20μm.

(C) Liver index (liver weight/body weight), ALT levels, and serum and liver Cholesterol or Triglyceride levels were measured in *Chil1*$^{fl/fl}$ and *Clec4f*$^{\Delta Chil1}$ mice fed a HFHC diet for 16 weeks. n=5 mice/group.

(D&E) *i.p.* glucose tolerance test (IGTT) and *i.p.* insulin tolerance test (ITT) were measured in *Chil1*$^{fl/fl}$ and *Clec4f*$^{\Delta Chil1}$ mice fed a HFHC diet for 16 weeks. n=5 mice/group.

Representative images are shown in A, B. Two-tailed, unpaired student t-test was performed in C, D, E. P value is as indicated.

Figure 3 ScRNA-seq reveals upregulated glucose metabolism-related transcripts in KCs, correlating with cell death signatures.

(A-D) Wildtype C57BL/6J mice were fed either a normal chow diet (NCD) or HFHC for 16 weeks. NPCs were isolated and subjected to BD Rhapsody scRNA sequencing.

(A) Quantification of each cell cluster is presented.

(B) KEGG analysis reveals the top 12 enriched pathways for up-regulated genes when comparing HFHC versus NCD in KCs, monocytes, and MoMFs, respectively.

(C) Gene set variation analysis (GSVA) shows pathway activity for cell death, glucose metabolism, and cell proliferation in KCs, monocytes, and MoMFs of WT mice fed NCD or HFHC for 16 weeks, respectively.

(D) The correlation between cell death and glucose metabolism pathways, based on GSVA score, is depicted.

Figure 4. Chi3l1 deficiency promote KCs death during MASLD.

(A) GSVA analysis showed the enrichment of cell death-related pathways in KCs from WT mice fed with either NCD or HFHC or *Chil1*$^{-/-}$ mice fed with HFHC.

(B) Dot plot showing the scaled gene expression levels of Apoptosis-related genes and repressor genes in KCs from either WT or *Chil1*$^{-/-}$ fed with HFHC.

(C) Flow cytometry analysis of CD45^{+} F4/80^{hi} CD11blow Timd4^{+} Kupffer cells on nonparenchymal liver cells (NPC) between WT and *Chil1*$^{-/-}$ mice.

(D) Number of KCs and MoMFs /liver or gram(g) liver were statistically analyzed. n= 3-4 mice per group.

(E) Immunofluorescent staining to detect Clec4f (green), Tunel (red), and nuclear DAPI (blue) in liver sections. Scale bar=20μm and 5μm(zoom). Tunel^{+} cells/Clec4f^{+} cells were statistically analyzed. n=3-4 mice/group.

Representative images are shown in C, E. One-way ANOVA was performed in D. Two-tailed, unpaired student t-test was performed in E. P value is as indicated.

Figure 5 Molecular interaction between Chi3l1 and glucose.

(A) A comparison of chemical structures between glucose and chitin.

(B) Prediction of Chi3l1-glucose interaction using STITCH database (http://stitch.embl.de).

(C) Strategy for pulling down glucose-binding proteins in murine serum.

(D) Biotin-conjugated glucose was incubated with murine serum from mice fed with HFHC for 16

weeks. Proteins bound to glucose were precipitated by streptavidin beads. Biotin or biotin-conjugated glucose plus glucose were used as negative controls. Western blot was performed to examine Chi3l1 in the precipitate.

(E) Microscale thermophoresis assay to detect the interaction between recombinant mouse Chi3l1 (rChi3l1) and glucose. Kd=4.95±0.66mM.

(F) Western blot to detect Chi3l1 expression in murine serum before and after HFHC feeding. n=3 mice/group.

Figure 6. Chi3l1 limits glucose uptake and protects hepatic macrophages from cell death.

(A) Following 12 h of glucose starvation, isolated KCs were divided into two groups: one treated with no 2-NBDG and the other with 2-NBDG. Within each group, KCs were further treated without or with recombinant murine Chi3l1 (rChi3l1) for 6 h. Glycogen aggregate formation labeled by 2-NBDG (Green) in BMDM was examined after counterstaining with nuclear DAPI (Blue). Scale bar=2μm.

(B) Following 12 h of glucose starvation, BMDM were divided into two groups: one treated with no 2-NBDG and the other with 2-NBDG. Within each group, BMDM were further treated without or with recombinant murine Chi3l1 (rChi3l1) for 6 h. Glycogen aggregate formation labeled by 2-NBDG (Green) in BMDM was examined after counterstaining with nuclear DAPI (Blue). Scale bar=2μm. The area of 2-NBDG-labeled aggregate foci was quantified.

(C) Following 12 h of glucose starvation, BMDM were treated with either no glucose or high glucose (25mM). Concurrently, BMDM were treated without or with rChi3l1 for 24 h under each condition. glycogen aggregate formation in BMDM was detected using immunofluorescence staining for Stbd1 (red) and nuclear DAPI (blue). Scale bar = 10 μm.

(D and E) BMDM cells were treated without or with rChi3l1 for 24 h and subjected to Seahorse metabolic analysis to measure the extracellular acidification rate (ECAR).

(F and G) KCs were treated without (blank) or with either Isopropyl alcohol(Iso) or 800uM palmitic acid (PA) or 100ng rChi3l1 with 800 uM PA for 24 h. Western blot was performed to detect cleaved caspase 3 (Cl-Casp3) in F. Calcein/PI staining was quantified to detect cell viability in G. Scale bar=50μm.

Representative images are shown in A-C. One-way ANOVA was performed in B, G. Two-tailed, unpaired student t-test was performed in E. P value is as indicated.

Figure 7. Differential regulation of KCs and MoMFs fate by Chi3l1-glucose interaction. KCs maintain a high-glucose activation state, while MoMFs exhibit a relatively low-glucose metabolic program. Chi3l1-glucose binding inhibits glucose uptake in KCs, thereby delaying KCs death and alleviating MASLD progression and metabolic dysfunction. In contrast, although Chi3l1-glucose binding similarly inhibits glucose uptake in MoMFs, their low basal glucose metabolism renders them resistant to this metabolic perturbation, resulting in minimal impact on MASLD pathogenesis

Figure 1

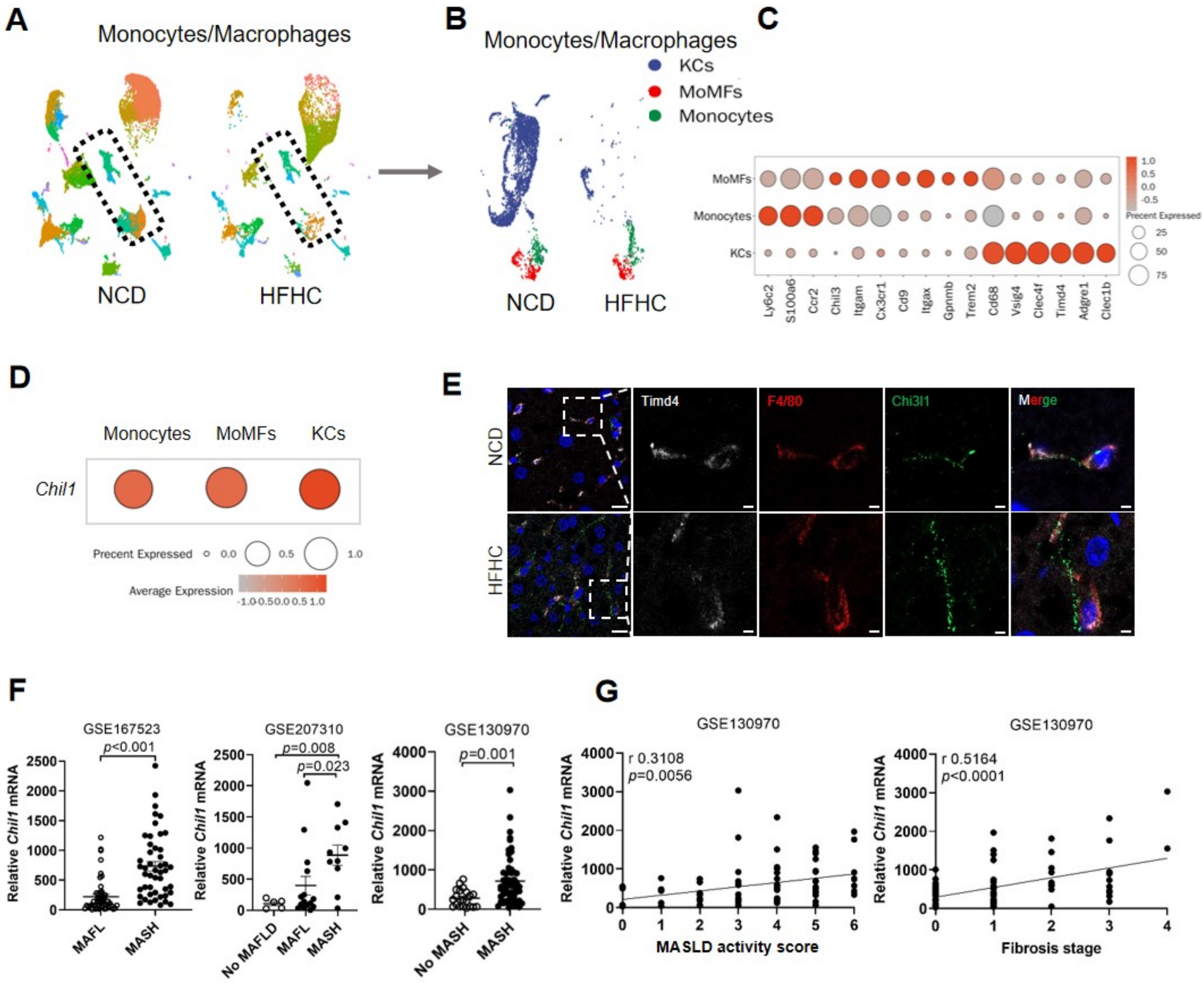
A
Monocytes/Macrophages
NCD
HFHC
B
Monocytes/Macrophages
KCs
MoMFs
Monocytes
NCD
HFHC
C
MoMFs
Monocytes
KCs
Ly6c2
S100a6
Ccr2
Chil3
Itgam
Cx3cr1
Cd9
Itgax
Gpnmb
Trem2
Cd68
Vsig4
Clec4f
Timd4
Adgre1
Clec1b
Precent Expressed
25
50
75
1.0
0.5
0.0
-0.5
D
Monocytes
MoMFs
KCs
Chil1
Precent Expressed
0.0
0.5
1.0
Average Expression
-1.0 -0.5 0.0 0.5 1.0
E
NCD
HFHC
Timd4
F4/80
Chi3l1
Merge
F
GSE167523
p<0.001
Relative Chil1 mRNA
MAFL
MASH
GSE207310
p=0.008
p=0.023
No MAFLD
MAFL
MASH
GSE130970
p=0.001
No MASH
MASH
G
GSE130970
r 0.3108
p=0.0056
MASLD activity score
GSE130970
r 0.5164
p<0.0001
Fibrosis stage

Figure 2

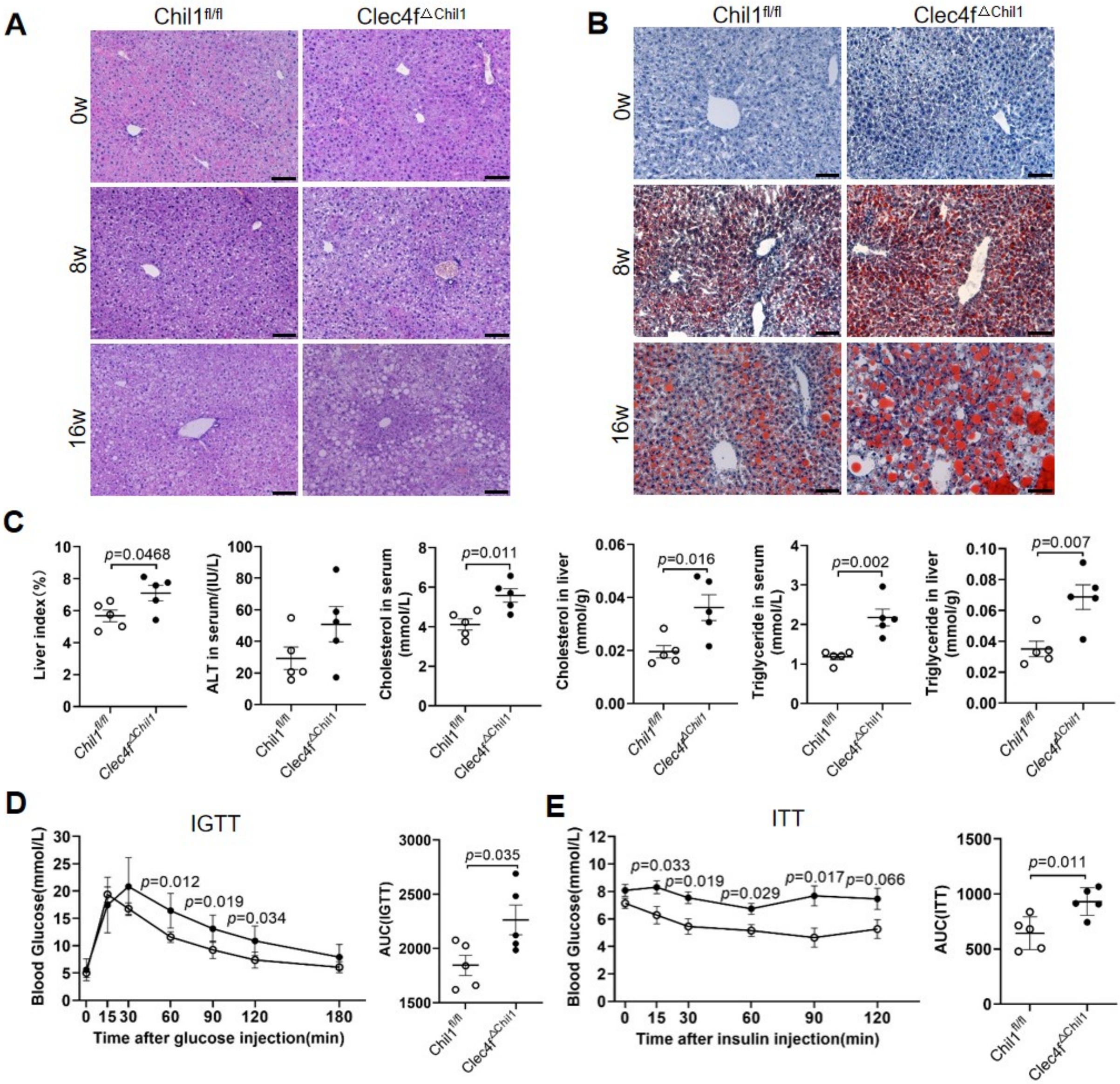
A
Chil1fl/fl
Clec4f△Chil1
0w
8w
16w
B
Chil1fl/fl
Clec4f△Chil1
0w
8w
16w
C
Liver index (%)
p=0.0468
ALT in serum/(IU/L)
Cholesterol in serum (mmol/L)
p=0.011
Cholesterol in liver (mmol/g)
p=0.016
Triglyceride in serum (mmol/L)
p=0.002
Triglyceride in liver (mmol/g)
p=0.007
Chil1fl/fl
Clec4f△Chil1
D
IGTT
Blood Glucose(mmol/L)
p=0.012
p=0.019
p=0.034
Time after glucose injection(min)
AUC(IGTT)
p=0.035
E
ITT
Blood Glucose(mmol/L)
p=0.033
p=0.019
p=0.029
p=0.017
p=0.066
Time after insulin injection(min)
AUC(ITT)
p=0.011

Figure 3

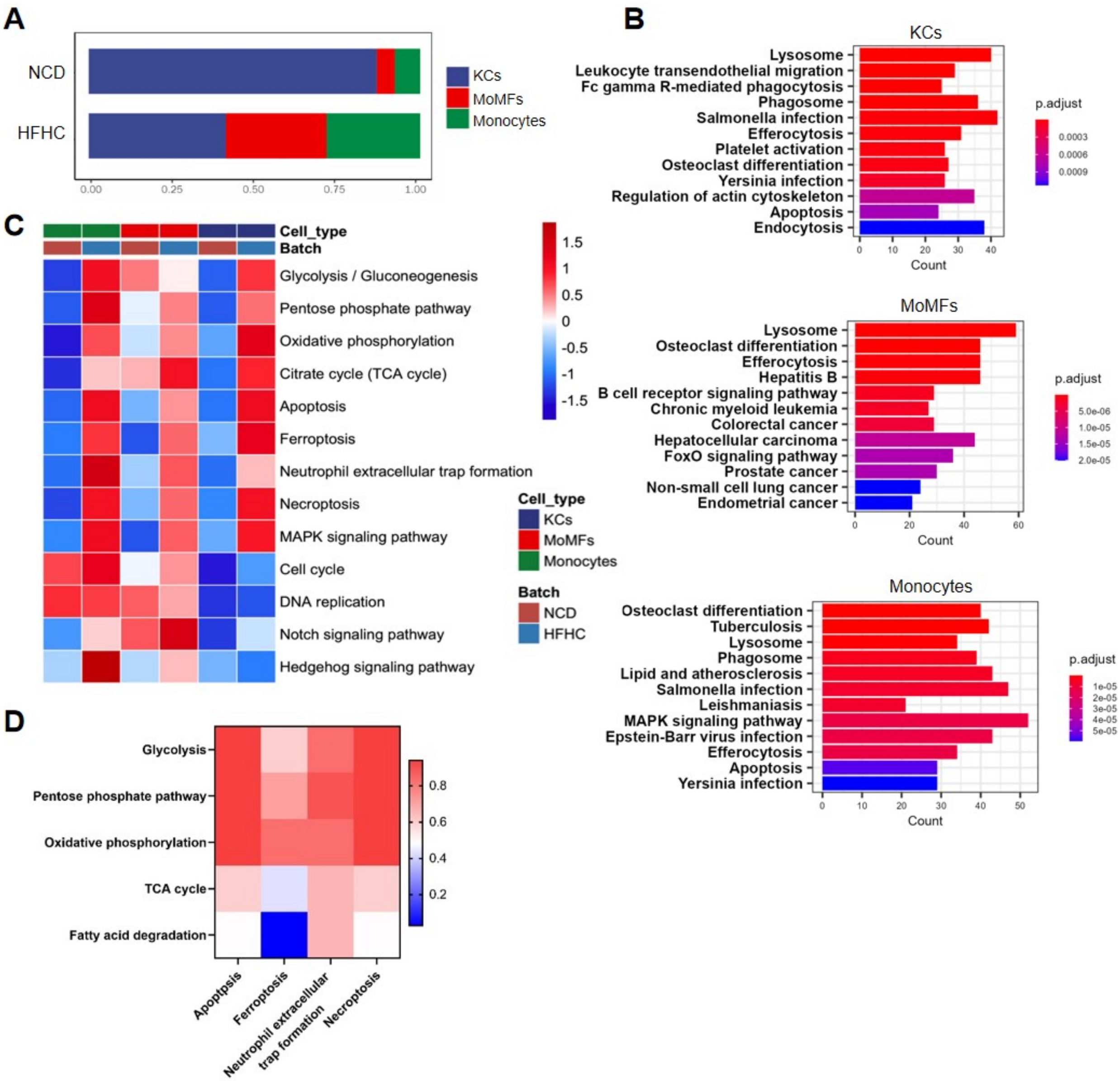
A
NCD
HFHC
0.00
0.25
0.50
0.75
1.00
KCs
MoMFs
Monocytes
B
KCs
Lysosome
Leukocyte transendothelial migration
Fc gamma R-mediated phagocytosis
Phagosome
Salmonella infection
Efferocytosis
Platelet activation
Osteoclast differentiation
Yersinia infection
Regulation of actin cytoskeleton
Apoptosis
Endocytosis
0
10
20
30
40
Count
p.adjust
0.0003
0.0006
0.0009
MoMFs
Lysosome
Osteoclast differentiation
Efferocytosis
Hepatitis B
B cell receptor signaling pathway
Chronic myeloid leukemia
Colorectal cancer
Hepatocellular carcinoma
FoxO signaling pathway
Prostate cancer
Non-small cell lung cancer
Endometrial cancer
0
20
40
60
Count
p.adjust
5.0e-06
1.0e-05
1.5e-05
2.0e-05
Monocytes
Osteoclast differentiation
Tuberculosis
Lysosome
Phagosome
Lipid and atherosclerosis
Salmonella infection
Leishmaniasis
MAPK signaling pathway
Epstein-Barr virus infection
Efferocytosis
Apoptosis
Yersinia infection
0
10
20
30
40
50
Count
p.adjust
1e-05
2e-05
3e-05
4e-05
5e-05
C
Cell_type
Batch
Glycolysis / Gluconeogenesis
Pentose phosphate pathway
Oxidative phosphorylation
Citrate cycle (TCA cycle)
Apoptosis
Ferroptosis
Neutrophil extracellular trap formation
Necroptosis
MAPK signaling pathway
Cell cycle
DNA replication
Notch signaling pathway
Hedgehog signaling pathway
1.5
1
0.5
0
-0.5
-1
-1.5
Cell_type
KCs
MoMFs
Monocytes
Batch
NCD
HFHC
D
Glycolysis
Pentose phosphate pathway
Oxidative phosphorylation
TCA cycle
Fatty acid degradation
Apoptpsis
Ferroptosis
Neutrophil extracellular trap formation
Necroptosis
0.8
0.6
0.4
0.2

Figure 4

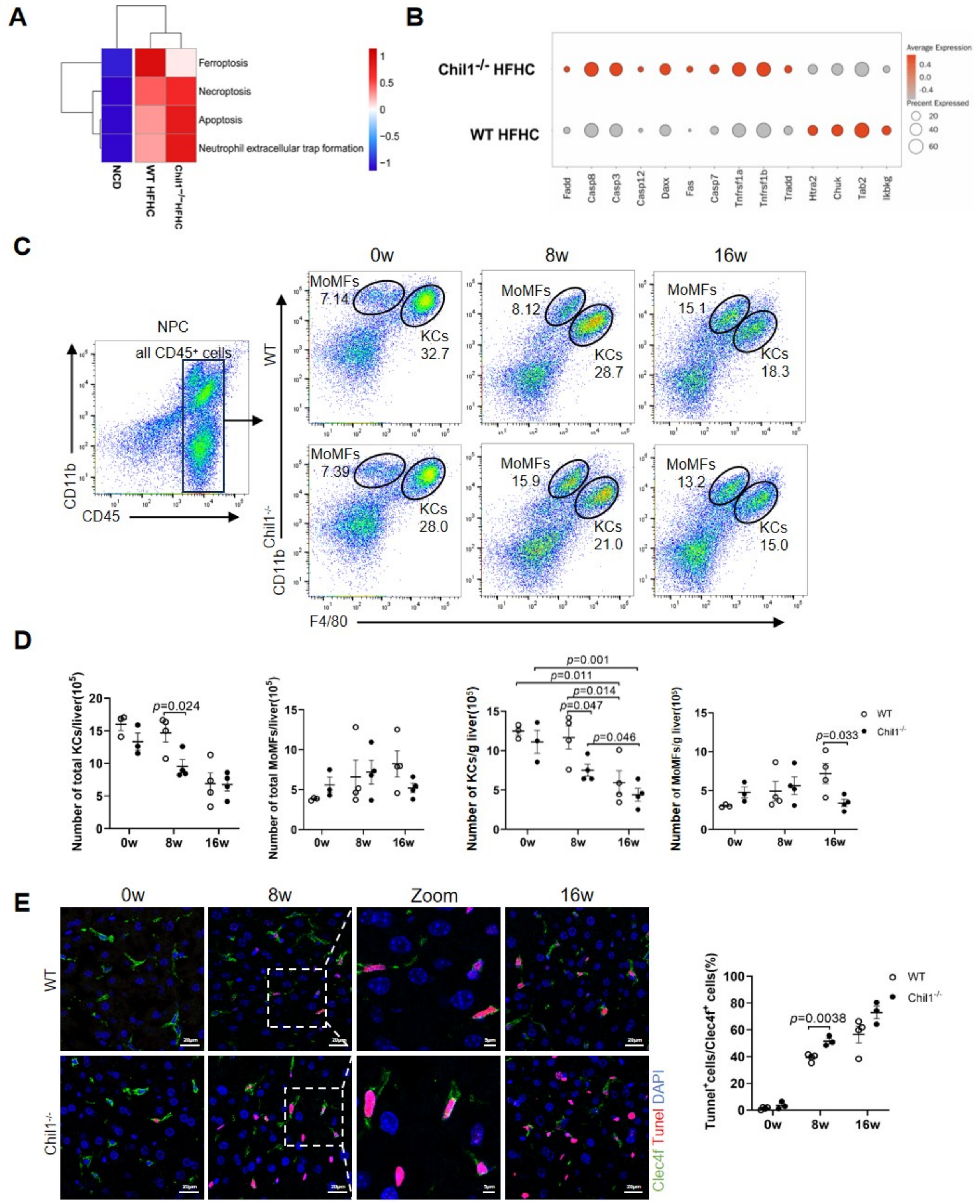
A
Ferroptosis
Necroptosis
Apoptosis
Neutrophil extracellular trap formation
NCD
WT HFHC
Chil1-/- HFHC
B
Chil1-/- HFHC
WT HFHC
Fadd
Casp8
Casp3
Casp12
Daxx
Fas
Casp7
Tnfrsf1a
Tnfrsf1b
Tradd
Htra2
Chuk
Tab2
Ikbkg
Average Expression
Precent Expressed
C
0w
8w
16w
NPC
all CD45+ cells
CD11b
CD45
WT
Chil1-/-
MoMFs 7.14
KCs 32.7
MoMFs 8.12
KCs 28.7
MoMFs 15.1
KCs 18.3
MoMFs 7.39
KCs 28.0
MoMFs 15.9
KCs 21.0
MoMFs 13.2
KCs 15.0
F4/80
D
Number of total KCs/liver(10^5)
p=0.024
Number of total MoMFs/liver(10^5)
Number of KCs/g liver(10^5)
p=0.001
p=0.011
p=0.014
p=0.047
p=0.046
Number of MoMFs/g liver(10^5)
p=0.033
WT
Chil1-/-
E
0w
8w
Zoom
16w
WT
Chil1-/-
Clec4f Tunel DAPI
Tunnel+cells/Clec4f+ cells(%)
p=0.0038

Figure 5

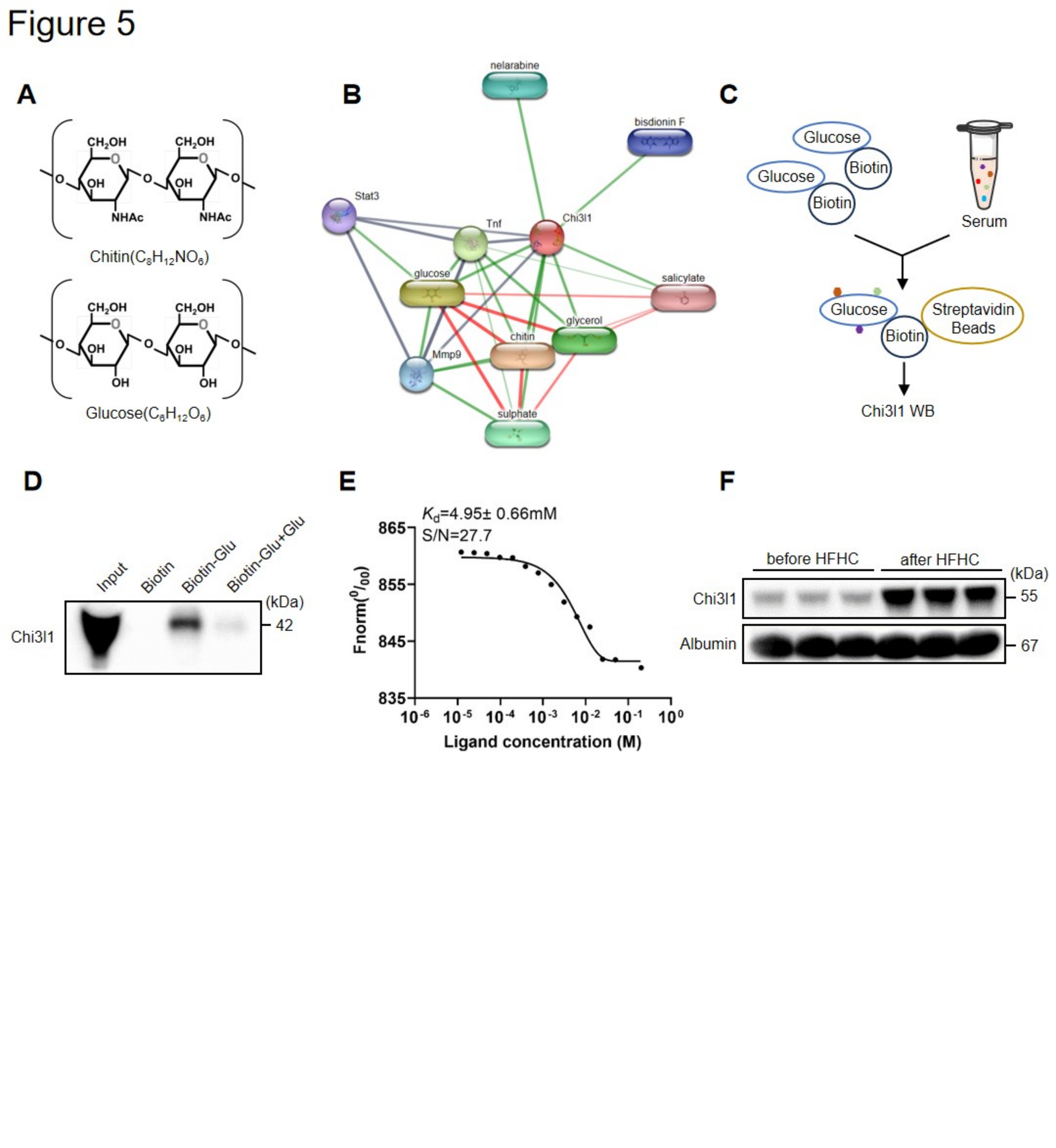
A
Chitin($C_8H_{12}NO_6$)
Glucose($C_6H_{12}O_6$)
B
nelarabine
bisdionin F
Stat3
Tnf
Chi3l1
glucose
salicylate
glycerol
chitin
Mmp9
sulphate
C
Glucose
Biotin
Serum
Streptavidin Beads
Chi3l1 WB
D
Input
Biotin
Biotin-Glu
Biotin-Glu+Glu
(kDa)
Chi3l1
42
E
K_d=4.95± 0.66mM
S/N=27.7
Fnorm(‰)
Ligand concentration (M)
F
before HFHC
after HFHC
(kDa)
Chi3l1
55
Albumin
67

Figure 6

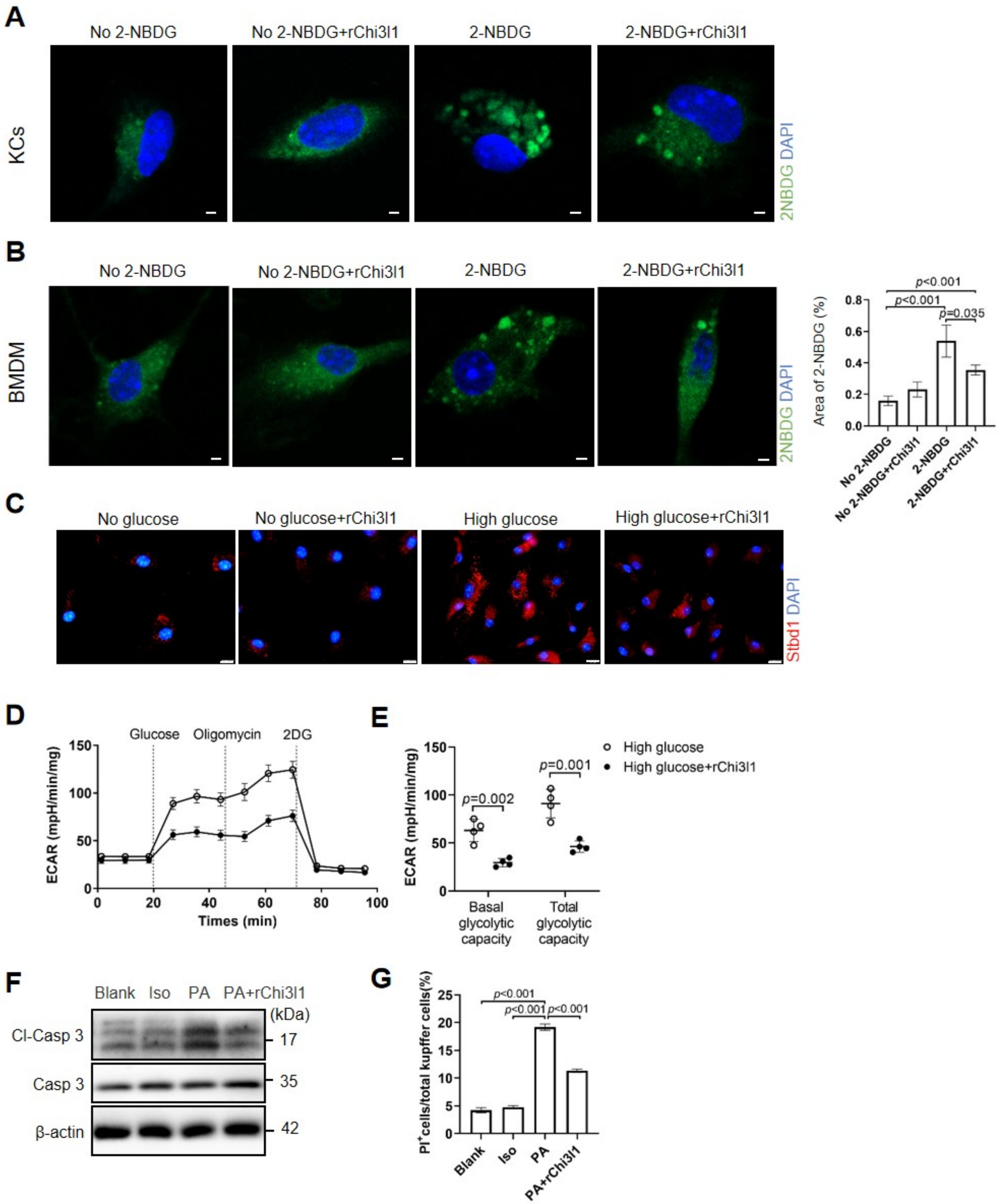
A
No 2-NBDG
No 2-NBDG+rChi3l1
2-NBDG
2-NBDG+rChi3l1
KCs
2NBDG DAPI
B
No 2-NBDG
No 2-NBDG+rChi3l1
2-NBDG
2-NBDG+rChi3l1
BMDM
2NBDG DAPI
p<0.001
p<0.001
p=0.035
Area of 2-NBDG (%)
0.0
0.2
0.4
0.6
0.8
No 2-NBDG
No 2-NBDG+rChi3l1
2-NBDG
2-NBDG+rChi3l1
C
No glucose
No glucose+rChi3l1
High glucose
High glucose+rChi3l1
Stbd1 DAPI
D
Glucose
Oligomycin
2DG
ECAR (mpH/min/mg)
0
50
100
150
0
20
40
60
80
100
Times (min)
E
High glucose
High glucose+rChi3l1
p=0.002
p=0.001
ECAR (mpH/min/mg)
0
50
100
150
Basal glycolytic capacity
Total glycolytic capacity
F
Blank
Iso
PA
PA+rChi3l1
(kDa)
Cl-Casp 3
17
Casp 3
35
β-actin
42
G
p<0.001
p<0.001
p<0.001
PI+cells/total kupffer cells(%)
0
5
10
15
20
25
Blank
Iso
PA
PA+rChi3l1

Figure 7

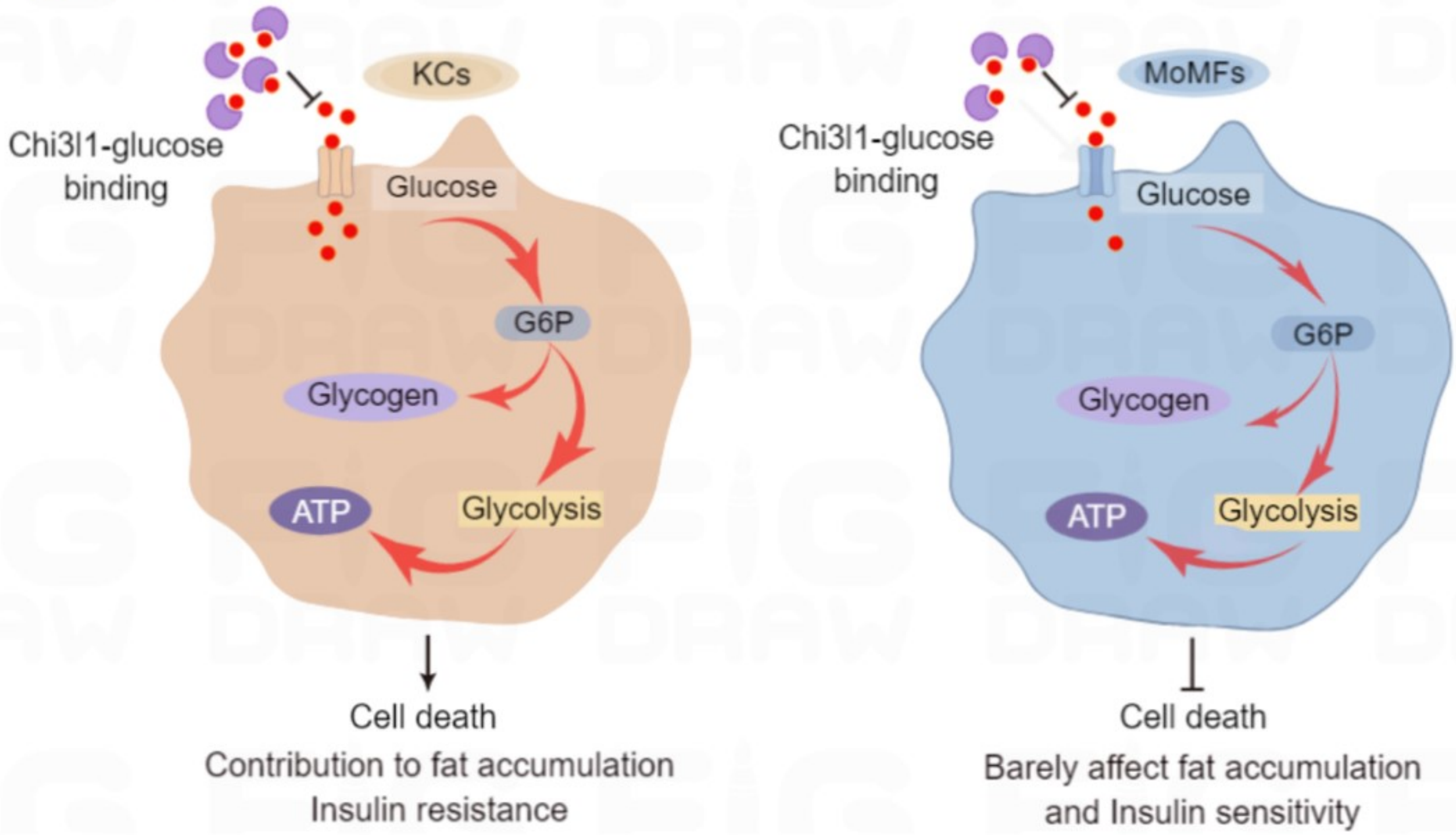
KCs
Chi3l1-glucose binding
Glucose
G6P
Glycogen
ATP
Glycolysis
Cell death
Contribution to fat accumulation
Insulin resistance
MoMFs
Chi3l1-glucose binding
Glucose
G6P
Glycogen
ATP
Glycolysis
Cell death
Barely affect fat accumulation
and Insulin sensitivity